Reconstructing the Local Potential of Inflation with BICEP2 data

Yin-Zhe Ma[1, 2, *] and Yi Wang[3, †]

[1]*Department of Physics and Astronomy, University of British Columbia, Vancouver, BC, V6T 1Z1, Canada*
[2]*Shanghai Astronomical Observatory, Chinese Academy of Science, 80 Nandan Road, Shanghai, China, 20003*
[3]*Centre for Theoretical Cosmology, DAMTP, University of Cambridge, Cambridge CB3 0WA, UK*

We locally reconstruct the inflationary potential by using the current constraints on r and $n_{\rm s}$ from BICEP2 data. Assuming small and negligible $\alpha_{\rm s}$, the inflationary potential is approximately linear in $\Delta\phi \sim M_{\rm pl}$ range but becomes non-linear in $\Delta\phi \sim 10 M_{\rm pl}$ range. However if we vary the value of $\alpha_{\rm s}$ within the range given by constraints from *Planck* measurement, the local reconstruction is only valid in the range of $\Delta\phi \sim 0.4 M_{\rm pl}$, which challenges the inflationary background from the point of view of effective field theory. We show that, within the range of $\Delta\phi \sim 0.4 M_{\rm pl}$, the inflation potential can be precisely reconstructed. With the current reconstruction, we show that $V(\phi) \sim \phi^2$ and ϕ^3 are consistent, while ϕ model is ruled out by 95% confidence level of the reconstructed range of potential. This sets up a strong limit of large-field inflation models.

I. INTRODUCTION

The Inflation paradigm [1, 2] is successful in explaining the horizon problem, flatness problem and the homogeneity problem in the standard hot-big-bang cosmology. The generic inflation model predicts a nearly scale-invariant primordial scalar power spectrum which has been measured accurately by the observations of the cosmic microwave background radiation (CMB) such as *Wilkinson Microwave Anisotropy Probe* (hereafter *WMAP*) [3] and *Planck* [4] satellites. However, even with precise constraints from CMB temperature fluctuations, there are still many models that predict the values of spectral index $n_{\rm s}$ and its running $dn_{\rm s}/d\ln k$ which are allowed by the constraints from current data.

Recently, the ground-based "Background Imaging of Cosmic Extragalactic Polarization" experiment just completed its second phase experiment (hereafter BICEP2), which observed the CMB B-mode polarization (divergence-free mode of polarization) on angular scales of a few degrees [5] (For cosmological implications, see also [6–9]). The CMB B-mode polarization can only be sourced by primordial gravitational waves, which is a very clean test of the primordial tensor fluctuations. Results from BICEP2 [5] show that the power spectrum of B-mode polarization C_ℓ^{BB} on a few degree angular scales is detected at $\sim 7\sigma$ confidence level (CL), which clearly indicates a signature of primordial gravitational waves. If this is true, it becomes a strong observational support of the scenario in which the Universe started from the inflationary exponential expansion, when the primordial tensor fluctuations are produced and stretched to super-Hubble length, and later entered into the Hubble horizon and decayed at small scales.

Indeed, this field of CMB observation has been developing very fast over the past decades and many on-going experiments are seeking such a CMB B-mode polarization signal. For instance, the *Planck* satellite with its nine frequency channels may achieve higher signal-to-noise ratio and probe even larger angular scales than BICEP2. Ground-based SPTPol [10], ACTPol [11], PolarBear [13] and CLASS [12] experiments are also completing with each other to make more precise measurement on the CMB B-mode polarization signals. Therefore further experiments may precisely determine not only the amplitude but also the shape of the primordial tensor power spectrum, therefore constitutes a direct test of the inflation mechanism.

Therefore it is important to connect the predictions from inflation models with the current observational results from BICEP2 and *Planck*. In pervious *WMAP* and *Planck* analysis papers [3, 14], the authors plot the predictions of spectral index of scalar power spectrum $n_{\rm s}$ and tensor-to-scalar ratio r of various inflation models with the constraints from CMB data (fig. 7 in [3] and fig. 1 in [14]). While making the prediction of $n_{\rm s}$–r relation for a given potential, the variation of the inflaton field is calculated by integrating the equation of motion from the end of inflation to some early epoch. This duration of inflation is assumed by to around 50–60 number of e-folds ($N = \log(a/a_{\rm i})$). Although the $n_{\rm s}$-r relation works well, it is worth noticing the underlying assumption that during inflation, the inflaton potential (which is typically taken as a monomial, for example, $V \propto \phi^2$) is the same as that during the first 10 e-folds of observable inflation.

---

*Electronic address: mayinzhe@phas.ubc.ca
†Electronic address: yw366@cam.ac.uk

With the recent measurement of tensor-to-scalar ratio r, this assumption become problematic. It becomes much more challenging than before to build an inflation model, in which a simple potential describes the total 60 e-folds of inflation without changing its shape and parameters. To see this, remember that the inflationary potential can be perturbatively expanded near a value of ϕ_* as

$$V(\phi) = V(\phi_*) + \partial_\phi V \Delta\phi + \cdots \frac{1}{4!}\partial_\phi^4 V \Delta\phi^4 + \cdots , \tag{1}$$

where $\Delta\phi = \phi - \phi_*$ is the change of ϕ value during inflation. From the effective field theory point of view, the potential derivatives up to $\partial_\phi^4 V$ are relevant and marginal operators. Those operators can be naturally turned on without suppression. On the other hand, the $\partial_\phi^4 V$ and higher derivatives are irrelevant operators, which are suppressed with an energy scale defined by the UV physics (at most the Planck scale). For the expansion (1) to converge we need $\Delta\phi$ to be smaller than the UV completion scale of inflation. However, Lyth bound [15] suggests that, the change of the field with respect to the number of e-folds is related to the value of r

$$\left|\frac{\mathrm{d}\phi}{\mathrm{d}N}\right| = \frac{M_{\mathrm{pl}}}{4}\sqrt{2r}, \tag{2}$$

where $M_{\mathrm{pl}} = (8\pi G)^{-1/2}$ is the reduced Planck mass. By substituting the current measurement of r from BICEP2 [5]

$$r = 0.20^{+0.07}_{-0.05} \ (1\sigma\mathrm{CL}). \tag{3}$$

Thus per e-fold, $\Delta\phi = 0.16 M_{\mathrm{pl}}$. By assuming $N \simeq 60$, we find that the inflaton field moves at least at a distance [1]

$$\Delta\phi \simeq 9.6 M_{\mathrm{pl}} , \tag{4}$$

in its field space. If this is true, $\Delta\phi$ at 60 e-folds is much greater than M_{pl}. Thus the expansion (1) is no-longer valid since all the high derivatives of V could in principle contribute along the 60 e-folds of the inflationary trajectory. The effective field theory of inflationary background is therefore non-perturbative, and becomes out of control for higher order derivatives.

The UV completion of inflation becomes a sharper problem then ever before. However, the leading UV completion paradigm, string theory, actually makes the problem worse. On the one hand, most string inflation models predict much smaller r and thus not consistent with the BICEP2 data. On the other hand, the characteristic energy scale of string theory is the string scale. For string theory to be perturbatively solvable, strong coupling had better to be small and the string scale should be lower than the Planck scale (say, 0.1 M_{pl} or lower). The size of extra dimension may further lower the string scale. With such a lower scale as the cutoff, the effective field becomes a greater challenge than that with the Planck scale cutoff.

Before BICEP2, the major challenge for building stringy inflation models is the η-problem [19], with the observational η smaller than theoretical expectations. Now, a more serious ϵ-problem emerges, leaving the observed large ϵ for the string theorists to explain.

In the effective field theory point of view, given the current constraint on r, we may not be able to trust the inflaton potential along the whole 60 number of e-folds. This motivates us not to integrate the potential throughout 60 number of e-folds, but to reconstruct the potential [20–22] locally. Therefore we focus on a local range of field values, along the first a few e-folds window. In this range, $\Delta\phi \sim M_{\mathrm{pl}}$ thus the inflationary potential expanded by Eq. (1) is in better control. We will show that, assuming small running, with current data it is possible to accurately reconstruct the amplitude and shape of the inflaton potential within the CMB observation window of about 10 e-folds. However, in the case of large running, the uncertainty of the reconstruction becomes large when $\Delta\phi$ is comparable with $0.4M_{\mathrm{pl}}$, which corresponds to a field range of about 3 e-folds.

This paper is organized as follows: in Sec. II, we explain our notations of slow-roll parameters, and show the connection with n_{s} and r. In Sec. III we directly constrain the slow-roll parameters with current data from BICEP2. In Sec. IV, we sample the inflationary potential and compare its amplitude and shape with the large-field inflation models. The conclusion and discussions are presented in the last section.

_____

[1] Here we do not take the time variation of ϵ into account, to avoid model dependence. Otherwise the number in (4) could change, while keep within the same order of magnitude. Also note that it is also possible that ϵ is not varying monotonically, to avoid large field inflation [16, 22].

II.   SLOW-ROLL PARAMETERS

The slow-roll parameters as derivatives of the scale factor can be defined as

$$\epsilon = -\frac{\dot{H}}{H^2} \ , \quad \eta = \eta_1 = \frac{\dot{\epsilon}}{H\epsilon} \ , \quad \eta_n = \frac{\dot{\eta}_{n-1}}{H\eta} \quad (n \geq 2) \ . \tag{5}$$

Note that these are equivalent to the parameters defined by the derivatives of the inflationary potential. However, the definitions (5) are increasingly commonly used and their role to keep track of the expansion history of inflation is by itself important.

The scalar power spectrum can be written as

$$P_\zeta = \frac{H^2}{8\pi^2 \epsilon M_{\rm pl}^2} \ , \tag{6}$$

where $M_{\rm pl} = 1/\sqrt{8\pi G} = 2.435 \times 10^{18} \text{GeV}$ is the reduced Planck mass. The spectral index of primordial power spectrum, the running of the spectral index and the tensor-to-scalar ratio for single-field slow-roll inflation is

$$n_{\rm s} - 1 = -2\epsilon - \eta \ , \tag{7}$$

$$\alpha_{\rm s} = -2\eta\epsilon - \eta\eta_2 \ , \tag{8}$$

$$r = 16\epsilon \ . \tag{9}$$

Given the current measurement of r (Eq. (3)) with $P_\zeta = 2.4 \times 10^{-9}$ at $k_0 = 0.05 \text{Mpc}^{-1}$ (best-fitting value constrained by *Planck* [14]), the best-fitting values of ϵ and Hubble parameter H are

$$\epsilon = 0.0125 \ , \quad H = 4.4 \times 10^{-5} M_{\rm pl} = 1.1 \times 10^{14} \text{GeV}, \tag{10}$$

respectively. This Hubble scale sets the energy scale of inflationary perturbations. The corresponding energy density is

$$\rho = 3M_{\rm pl}^2 H^2 = 2.0 \times 10^{-9} M_{\rm pl}^4 = (1.6 \times 10^{16} \text{GeV})^4 \ , \tag{11}$$

which is about 10^{12} times higher than the current Large Hadron Collider (LHC) experiment. Therefore, the CMB experiment is essentially a high-energy experiment that probes the regime of physics inaccessible by the current ground-based accelerators.

Note that $\rho^{1/4}$ is of order the maximal temperature that the universe could get at reheating. The current preferred value $\sim 10^{16} \text{GeV}$ is interestingly near the grand unification scale. It thus becomes increasingly important to understand the relation between inflation and the grand unification, including model building, reheating mechanism, and possible topological defects which might be produced at the grand unification phase transition.

The tensor power spectrum and its spectral index are

$$P_{\rm T} = \frac{2H^2}{\pi^2 M_{\rm pl}^2} = 4.8 \times 10^{-10} \ , \tag{12}$$

$$n_{\rm T} = -2\epsilon = -\frac{r}{8} = -0.025 \ , \tag{13}$$

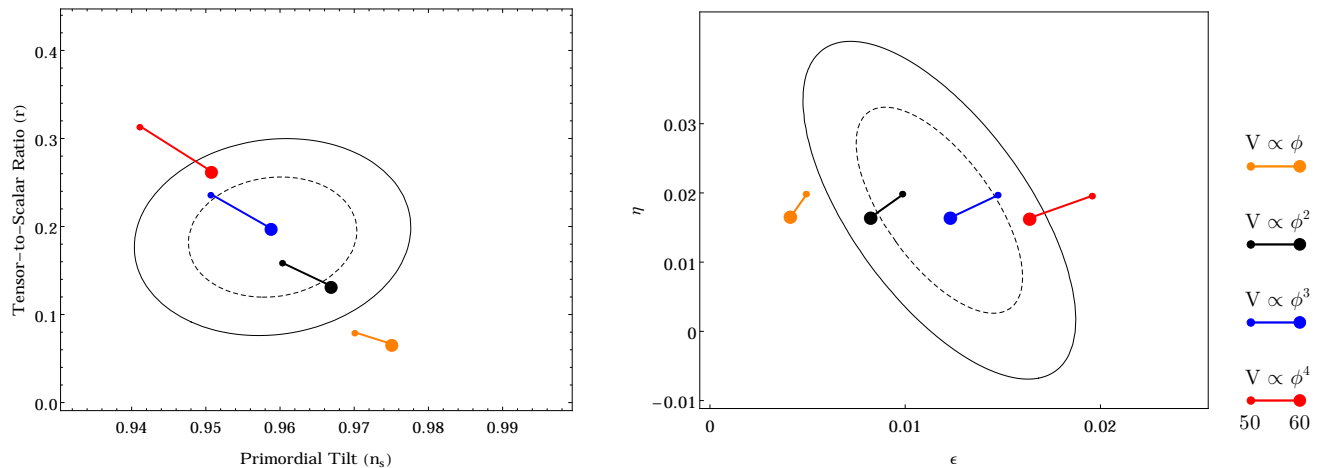where the second equation holds only for single-field slow-roll inflation models.

FIG. 1: *Left*– Joint constraint on n_s and r from *Planck*+WP+highL+BICEP2 data [5]. *Right*– The derived equal-probability contours on the ϵ-η plane. In both two panels, the dashed and solid lines are the 68.3% and 95.4% confidence level respectively.

III.   RECONSTRUCTION OF THE SLOW-ROLL PARAMETERS

Figure 1 shows the joint constraints ($1, 2\sigma$ confidence level) on n_s–r with current *Planck*+ WP [2]+ highL [3] + BICEP2. We have also plotted together the prediction of n_s–r relation during the number of e-folds $N = 50$–60, for the large-field inflation models $V \propto \phi^n$, (n=1,2,3,4) (see Sec. V for details). We can see that the ϕ^2 and ϕ^3 are within or near the 68.3% CL (depending on e-folds), and the previously considered "ruled out" ϕ^4 potential is now back inside 95.4% contour if $N \simeq 60$. The linear potential becomes disfavored by the new data.

The n_s-r diagram can be fitted by the multivariate normal distribution

$$L(n_\mathrm{s}, r) = \frac{1}{2\pi\sqrt{1 - \rho_{nr}^2}\,\sigma_n \sigma_r} \exp\left\{ -\frac{1}{2(1 - \rho_{nr}^2)} \left[\frac{(n_\mathrm{s} - 1 - \mu_n)^2}{\sigma_n^2} + \frac{(r - \mu_r)^2}{\sigma_r^2} - 2\frac{(n_\mathrm{s} - 1 - \mu_n)(r - \mu_r)\rho_{nr}}{\sigma_n \sigma_r} \right] \right\} \, , \quad (14)$$

where μ_n, σ_n (μ_r, σ_r) are the central value and standard deviation of $n_\mathrm{s} - 1$ (r) respectively. The ρ_{nr} is their correlation coefficient. Fitting this multi-variant Gaussian distribution with the (n_s, r) diagram (Fig. 1), we find

$$\mu_n = -0.041 \, , \quad \sigma_n = 0.0075 \, , \quad \mu_r = 0.19 \, , \quad \sigma_r = 0.045 \, , \quad \rho_{nr} = 0.10 \, . \quad (15)$$

The equal-probability contours of multivariate distribution are those with the exponent

$$e_{nr} \equiv \frac{1}{(1 - \rho_{nr}^2)} \left[\frac{(n_\mathrm{s} - 1 - \mu_n)^2}{\sigma_n^2} + \frac{(r - \mu_r)^2}{\sigma_r^2} - 2\frac{(n_\mathrm{s} - 1 - \mu_n)(r - \mu_r)\rho_{nr}}{\sigma_n \sigma_r} \right] = \text{constant} \, . \quad (16)$$

The e_{nr} as a random variable obeys $(\chi_2)^2$ distribution (i.e. the χ^2 distribution with two degrees of freedom). A contour with probability α inside the contour corresponds to

$$e_{nr} = 2\log\left(\frac{1}{1 - \alpha} \right) \, . \quad (17)$$

From (7) and (9), the inflationary slow-roll parameters ϵ and η satisfies the multivariate normal distribution

$$L(\epsilon, \eta) = \frac{1}{2\pi\sqrt{1 - \rho_{\epsilon\eta}^2}\,\sigma_\epsilon \sigma_\eta} \exp\left\{ -\frac{1}{2(1 - \rho_{\epsilon\eta}^2)} \left[\frac{(\epsilon - \mu_\epsilon)^2}{\sigma_\epsilon^2} + \frac{(\eta - \mu_\eta)^2}{\sigma_\eta^2} - 2\frac{(\epsilon - \mu_\epsilon)(\eta - \mu_\eta)\rho_{\epsilon\eta}}{\sigma_\epsilon \sigma_\eta} \right] \right\} \, , \quad (18)$$

---

[2] This is the *WMAP* polarization data [3].
[3] This high-ℓ CMB data is mainly from 150GHz South Pole Telescope (SPT) [17] and 148GHz Antacama Cosmology Telescope (ACT) [18].

with the central value, standard deviation and the correlation coefficient of ϵ and r being

$$\mu_\epsilon = \frac{\mu_r}{16} \ , \quad \sigma_\epsilon = \frac{\sigma_r}{16} \ , \tag{19}$$

$$\mu_\eta = -\mu_n - \frac{\mu_r}{8} \ , \quad \sigma_\eta = \frac{1}{8}\sqrt{64\sigma_n^2 + 16\rho\sigma_n\sigma_r + \sigma_r^2} \ , \tag{20}$$

$$\rho_{\epsilon\eta} = \frac{\left(\rho_{nr}^2 - 1\right)\sigma_r - \rho_{nr}\left|8\sigma_n + \rho_{nr}\sigma_r\right|}{\sqrt{16\sigma_n\rho_{nr}\sigma_r + 64\sigma_n^2 + \sigma_r^2}}. \tag{21}$$

Plugging in the data from (15), we obtain

$$\mu_\epsilon = 0.012 \ , \quad \sigma_\epsilon = 0.0028 \ , \quad \mu_\eta = 0.018 \ , \quad \sigma_\eta = 0.0098 \ , \quad \rho_{\epsilon\eta} = -0.65 \ . \tag{22}$$

The 68.3% and 95.4% CL of the joint constraints ϵ and η are plotted in the right panel of Fig. 1. One can see that the constraints on large-field inflation is the same as the left panel of Fig. 1: the ϕ^2 and ϕ^3 models are favoured by the current data within 2σ CL, while ϕ^1 model is ruled out at 2–3σ CL.

The probability distribution of η_2, on the other hand, can be derived from the current bound of α_s. Current data shows [23]

$$\alpha_s = -0.022 \pm 0.010 \quad (68\%\text{CL}) \ . \tag{23}$$

To good precision, one can approximate $\eta_2 = -\alpha_s/\eta$, considering that $2\eta\epsilon$ is much smaller than the current experimental bound.

On the other hand, for most slow-roll models of inflation, η_2 is much smaller than the current bound. Here we shall assume η_3 and η_4 are of the order η or smaller, while consider both cases of large η_2 and small η_2, motivated by observations and theory respectively.

IV.   RECONSTRUCTION OF THE INFLATIONARY POTENTIAL

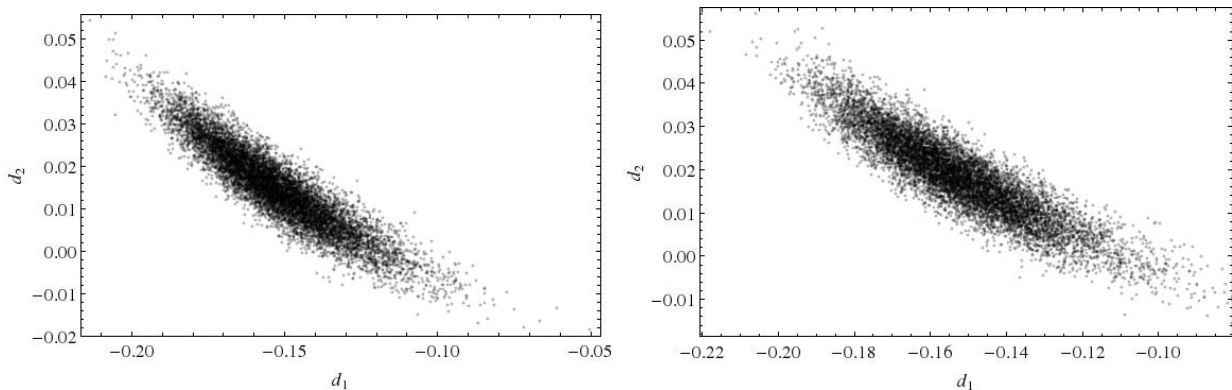### A.   Derivatives of the Inflationary Potential

FIG. 2: The probability distribution of d_1 and d_2. Here 10^4 points are dropped to illustrate the distribution in both panels. *Left*– Assuming that α_s is small and negligible. *Right*– Treating α_s as a free parameter and using the observational constraint α_s (Eq. (23)) to reconstruct d_1–d_2. As one can find (and analytically expect), the dependence on α_s is weak for d_1 and d_2.

In this section we expand the inflationary potential in terms of the slow-roll parameters. Since we are only interested in the range of a few number of e-folds, we are able to locally expand the potential in an effective field theory and have more confident to drop the non-renormalizable terms. In addition, higher order derivatives on the potential are highly suppressed by slow-roll parameters (and by the largeness of $M_{\rm pl}$) practically (unless the higher order slow-roll parameters are unusually huge). Thus we derive the derivatives of the potential up to 4th order.

In single field inflation (without slow-roll approximation), the derivatives of the potential can be solved from the slow-roll parameters as

$$\partial_\phi V = \frac{1}{2}H(-6 + 2\epsilon - \eta)\dot{\phi}, \tag{24}$$

$$\partial_\phi^2 V = -\frac{1}{4}H^2\left(8\epsilon^2 - 2\epsilon(12 + 5\eta) + \eta\left(6 + \eta + 2\eta_2\right)\right), \tag{25}$$

$$M_{\rm pl}^2 \partial_\phi^3 V = \frac{H\dot{\phi}\left(8\epsilon^3 - 6\epsilon^2(4 + 3\eta) + \epsilon\eta\left(18 + 6\eta + 7\eta_2\right) - \eta\eta_2\left(3 + \eta + \eta_2 + \eta_3\right)\right)}{4\epsilon}, \tag{26}$$

$$M_{\rm pl}^2 \partial_\phi^4 V = -4H^2\epsilon^3 + 2H^2\epsilon^2(6 + 7\eta) - \frac{1}{4}H^2\epsilon\eta\left(72 + 39\eta + 32\eta_2\right)$$

$$+ \frac{1}{8}H^2\eta\left(6\eta^2 + \eta\left(18 + 35\eta_2\right) + 6\eta_2\left(8 + 3\eta_2 + 3\eta_3\right)\right)$$

$$+ \frac{H^2\eta\eta_2\left(\eta^2 - \eta\left(-3 + 3\eta_2 + \eta_3\right) - 2\left(\eta_2^2 + 3\eta_2\left(1 + \eta_3\right) + \eta_3\left(3 + \eta_3 + \eta_4\right)\right)\right)}{8\epsilon} \tag{27}$$

Slow-roll approximation simplifies the above equations. However, it is important to note that if we allow large running, η_2 could be as large as $\mathcal{O}(1)$. Thus here we perform slow-roll approximation, but leaves η_2 not approximated [4]. By using $\dot{\phi} = M_{\rm pl}H\sqrt{2\epsilon}$, Eqs. (25–27) can be simplified as

$$d_0 \equiv \frac{V}{3M_{\rm pl}^2 H^2} \simeq 1 \,, \tag{28}$$

$$d_1 \equiv \frac{M_{\rm pl}}{V}\partial_\phi V \simeq -\sqrt{2\epsilon} \,, \tag{29}$$

$$d_2 \equiv \frac{M_{\rm pl}^2}{V}\partial_\phi^2 V \simeq \frac{1}{2}\left(4\epsilon - \eta - \frac{1}{3}\eta\eta_2\right) \,, \tag{30}$$

$$d_3 \equiv \frac{M_{\rm pl}^3}{V}\partial_\phi^3 V \simeq -\frac{\left(8\epsilon^2 - 6\epsilon\eta(1 + 7\eta_2/18) + \eta\eta_2(1 + (\eta + \eta_2 + \eta_3)/3)\right)}{\sqrt{2\epsilon}} \,, \tag{31}$$

$$d_4 \equiv \frac{M_{\rm pl}^4}{V}\partial_\phi^4 V \simeq \frac{\eta\eta_2\left(-2\eta_2^2 + \eta(\eta + 3) - 64\epsilon^2 + (35\eta + 48)\epsilon + 3\eta_2\left(-\eta - 2\eta_3 + 6\epsilon - 2\right) - \eta_3\left(\eta + 2\eta_3 + 2\eta_4 - 18\epsilon + 6\right)\right)}{24\epsilon}$$

$$+ \frac{\epsilon\left(3\eta^2 + 16\epsilon^2 - 24\eta\epsilon\right)}{4\epsilon} \,, \tag{32}$$

where dimensionless parameters d_i ($i = 0, 1, 2, 3, 4$) are defined to measure the derivatives of the inflationary potential. Without loss of generality we have used $\dot{\phi} = \sqrt{2\epsilon}M_{\rm pl}H > 0$, i.e. we have chosen the positive sign solution instead of the negative sign solution $\dot{\phi} = -\sqrt{2\epsilon}M_{\rm pl}H < 0$. This is because given a potential with a $\dot{\phi} < 0$ solution, one can always flip the potential by $\phi \to -\phi$ redefinition without change of any physics.

With the definition in (28), d_n is of order $\mathcal{O}(\epsilon, \eta_i)^{n/2}$ in slow-roll parameters. However, one should note that there may be a hierarchy between ϵ and η such that the above counting ($\mathcal{O}(\epsilon, \eta_i)^{n/2}$) may break down if $\epsilon \ll \eta$. Fortunately, with the current tensor we should have at least $\epsilon \sim \eta$. Thus the slow-roll order counting should be fine unless fine tuning happens.

With the above definition, the potential can be reconstructed till 4th order as

$$V(\phi) \simeq V(\phi_*)\left[1 + d_1\left(\frac{\Delta\phi}{M_{\rm pl}}\right) + \frac{1}{2}d_2\left(\frac{\Delta\phi}{M_{\rm pl}}\right)^2 + \frac{1}{6}d_3\left(\frac{\Delta\phi}{M_{\rm pl}}\right)^3 + \frac{1}{24}d_4\left(\frac{\Delta\phi}{M_{\rm pl}}\right)^4\right] \,. \tag{33}$$

Here one can see explicitly that if $\Delta\phi > M_{\rm pl}$, the coefficients d_n are required to be smaller for higher orders in order for the Taylor expansion to be converged.

---

[4] The calculation of P_ζ, $n_{\rm s} - 1$ and $\alpha_{\rm s}$ around local potential does not rely on the smallness of η_2. See, for example, [24], for the computational details. This is an advantage of making use of the slow roll parameters defined from expansion. On the other hand, if the slow roll parameters are defined by derivatives of the potential, the large η_2 enters the calculation, though eventually cancelled in calculating the observables.

B. Sampling the Inflationary Potential

Before performing the numerical reconstruction of potential, we derive a few analytical relations. Given the distribution of ϵ and η, the statistical properties of d_1 and d_2 can be calculated as

$$\mu_1 \equiv \langle d_1 \rangle = -\frac{i\left(\sqrt{2}\Gamma\left(\frac{3}{4}\right)\sigma_\epsilon \, {}_1F_1\left(-\frac{1}{4};\frac{1}{2};-\frac{\mu_\epsilon^2}{2\sigma_\epsilon^2}\right) - 2\Gamma\left(\frac{5}{4}\right)\mu_\epsilon \, {}_1F_1\left(\frac{1}{4};\frac{3}{2};-\frac{\mu_\epsilon^2}{2\sigma_\epsilon^2}\right)\right)}{2^{3/4}\sqrt{\pi}\sqrt{\sigma_\epsilon}}$$

$$- \frac{\sqrt{\pi}\mu_\epsilon^{3/2}e^{-\frac{\mu_\epsilon^2}{4\sigma_\epsilon^2}}I_{-\frac{1}{4}}\left(\frac{\mu_\epsilon^2}{4\sigma_\epsilon^2}\right)}{4\sigma_\epsilon} - \frac{\sqrt{\pi}\mu_\epsilon^{3/2}e^{-\frac{\mu_\epsilon^2}{4\sigma_\epsilon^2}}I_{\frac{3}{4}}\left(\frac{\mu_\epsilon^2}{4\sigma_\epsilon^2}\right)}{4\sigma_\epsilon} - \frac{\sqrt{\pi}\mu_\epsilon^{3/2}e^{-\frac{\mu_\epsilon^2}{4\sigma_\epsilon^2}}I_{\frac{5}{4}}\left(\frac{\mu_\epsilon^2}{4\sigma_\epsilon^2}\right)}{4\sigma_\epsilon}$$

$$- \frac{\sqrt{\pi}e^{-\frac{\mu_\epsilon^2}{4\sigma_\epsilon^2}}\left(\mu_\epsilon^2+2\sigma_\epsilon^2\right)I_{\frac{1}{4}}\left(\frac{\mu_\epsilon^2}{4\sigma_\epsilon^2}\right)}{4\sqrt{\mu_\epsilon}\sigma_\epsilon} + \frac{4\mu_\epsilon^{3/2}\,{}_2F_2\left(\frac{1}{2},1;\frac{5}{4},\frac{7}{4};-\frac{\mu_\epsilon^2}{2\sigma_\epsilon^2}\right)}{3\sqrt{\pi}\sigma_\epsilon} \ , \tag{34}$$

$$\sigma_1^2 \equiv \langle d_1^2 \rangle - \mu_1^2 = 2\mu_\epsilon - \mu_1^2 \ , \tag{35}$$

$$\mu_2 \equiv \langle d_2 \rangle = 2\mu_\epsilon - \frac{\mu_\eta}{2} \ , \tag{36}$$

$$\sigma_2^2 \equiv \langle d_2^2 \rangle - \mu_2^2 = 4\sigma_\epsilon - 2\rho_{\epsilon\eta}\sigma_\epsilon\sigma_\eta + \frac{\sigma_\eta^2}{4} \ . \tag{37}$$

where ${}_pF_q$ is the hypergeometric function and I_ν is the modified Bessel function of the first kind.

For the calculation of μ_2 and σ_2, we have assumed that η_2 is small and negligible. However, in the following numerical sampling, we shall consider both possibilities: either sampling η_2 from observational bound of α_s, or assuming η_2 is small and negligible.

First(and also theoretically reasonable), we can assume that η_n $(n \geq 2)$ are random variables with the same variance as η (a difference at the same order of magnitude does not change the result significantly). The probability distribution of d_3 and d_4 are plotted in the left panel of Fig. 3. From the plot, we confirm that with the mild theoretical assumptions discussed before, the derivative expansion of the potential converges nicely as a local expansion. We have also checked our assumption of the η_3 and η_4 distribution in the middle panel of Fig. 3, where η_3 and η_4 are set to zero, which does not significantly modify the distribution of d_3 and d_4.

Second, we also assume non-zero α_s and take its constraints (Eq. (23)) (the values near the observational bound) to sample the potential. This possibility seems not very probable theoretically. But on the other hand, observationally a large α_s would be the easiest way to resolve the tension between the low r reported by *WMAP/Planck*, and the high r reported by BICEP2. The tension may either be resolved by considering isocurvature perturbations or the anomalous suppression of power at low ℓ. But those possibilities are beyond the scope of the current work.

The distribution of d_1 and d_2 is illustrated in Fig. 2, with small α_s and observational α_s respectively. As one can find (and analytically expect), the dependence on α_s is weak for d_1 and d_2.

In right panel of Fig. 3, we use α_s to constrain η_2. There η_3 and η_4 are treated as having a variance the same as η. But the choice of η_3 and η_4 only affects d_4, which is the least important one in the reconstruction.
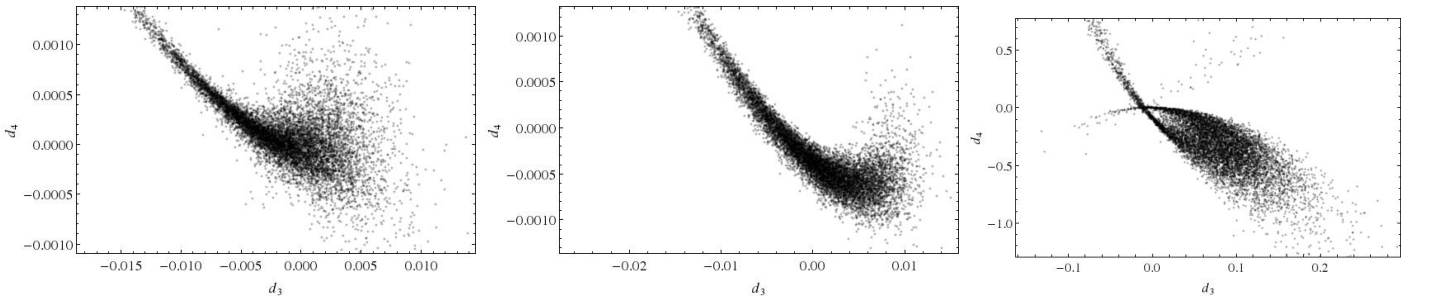

FIG. 3:   The probability distribution of d_3 and d_4. In each panel there are 10^4 random numbers chosen to sample the distribution. *Left*–η_2, η_3 and η_4 are assumed to be random variables with the same mean and variance of η. Unlike the (d_1, d_2) plot, the central value of d_3 and d_4 are around zero while the distribution is highly distorted. *Middle*– η_2, η_3 and η_4 set to zero. Comparing with left panel, the statistical properties are not significantly modified without or with small η_2, η_3 and η_4. *Right*– η_2 is determined by the constraint on α_s (Eq. (23)). Since the error of α_s is still quite significant, the parameter space is broadened by orders of magnitude.

Finally, with the realizations of d_1, d_2, d_3 and d_4, we can reconstruct $V(\phi)$ locally from (33). The reconstruction is plotted in Fig. 4, for $\alpha_s = 0$ case (left panel) and large α_s case (right panel) respectively.

For the case of $\alpha_s = 0$, the reconstructed potential is highly linear within the range $\Delta\phi \sim M_{\rm pl}$. But when we extrapolate the potential into about $10M_{\rm pl}$ range, which is suggested by large field inflation, we see higher order derivatives does tend to bend the reconstructed potential.

In the large α_s case, the reconstructed potential has significant non-linearities at $\Delta\phi > 0.2M_{\rm pl}$, especially for exceptional values of d_n in the parameter space. On the other hand, we are still fine for a local range of $\Delta\phi \simeq 0.4M_{\rm pl}$.
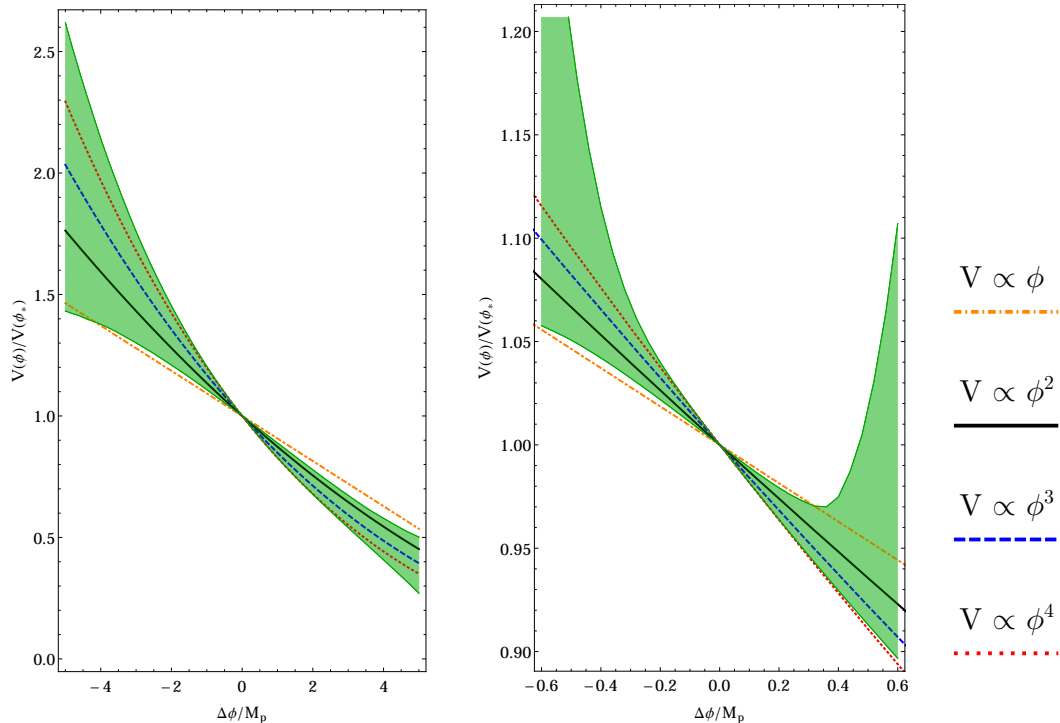

FIG. 4: The local reconstruction of the inflationary potential. The green shaded region is the 2σ region which contains 95% of the sampling points. In both panels, 3×10^4 points are dropped to calculate $\Delta\phi$.
Left– Without using constraint on α_s but instead assuming that η_2, η_3 and η_4 have the same variance as η (and checked that the shape of the potential does not change much for other distributions of those variables, as long as their variances are small). *Right*– Using the constraint of α_s (Eq. (23)) to determine the distribution of η_2. Also assuming that η_3 and η_4 has the same variance as η.

V. COMPARING THE LARGE-FIELD INFLATION MODELS WITH DATA

Although the local reconstruction of the inflaton potential is safer than fitting a global potential, but nevertheless considering the global inflationary potential by one polynomial function is very widely used, here we compare our local reconstruction with the global inflaton potential $V = \lambda\phi^n$.

The detailed analysis of the reheating history is beyond the scope of the current paper. Here we use the analytical approximation that inflation ends when $\epsilon = 1$, and use slow-roll approximation before reaching $\epsilon = 1$. In this approach, $\epsilon = 1$ corresponds to $\phi_{\rm end} = M_{\rm pl}n/\sqrt{2}$. The relevant quantities at horizon crossing can be calculated as

$$\phi_* = M_{\rm pl}\sqrt{2nN + \frac{n^2}{2}} \ , \qquad \epsilon = \frac{n}{4N + n} \ , \qquad \eta = \frac{4}{4N + n} \ . \tag{38}$$
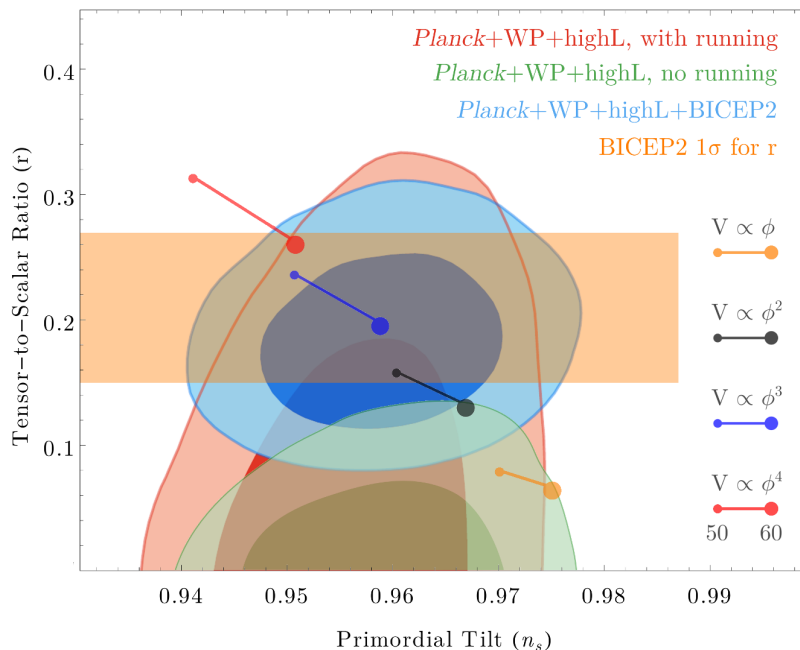
FIG. 5: n_{s}–r diagram with predictions of $V(\phi) \sim \phi, \phi^2, \phi^3, \phi^4$ models and the joint constraints. The *Planck*+WP+highL plots with and without running are extracted from [23]. The BICEP2 1σ result and its combined analysis with *Planck*+WP+highL (with running) are taken from [5]. Note that the large field inflation models do not have large running. Thus the matching between those inflation models and the two of those four contours which are marginalized with running should not be over interpreted (we thank Daniel Baumann for pointing it out).

Those values corresponds to

$$
P_\zeta = \frac{(4N+n)\lambda \left(M_{\text{pl}}\sqrt{2nN+\frac{n^2}{2}}\right)^n}{24n\pi^2 M_{\text{pl}}^4} \ , \quad n_{\text{s}} - 1 = -\frac{2(n+2)}{4N+n} \ , \quad r = \frac{16n}{4N+n} \ . \tag{39}
$$

The corresponding parameters are plotted on the n_s-r diagram in Fig. 5

Currently, the best models which fits the BICEP2 data is the ϕ^2 and ϕ^3 models. From the power spectrum, λ for those models are (note that the power spectrum is calculated at $k = 0.002\text{Mpc}^{-1}$)

$$
\lambda = 3.1 \times 10^{-11} M_{\text{pl}}^2 \quad (\phi^2, N = 50) \ , \quad \lambda = 1.8 \times 10^{-12} M_{\text{pl}} \quad (\phi^3, N = 50) \ , \tag{40}
$$

and

$$
\lambda = 2.1 \times 10^{-11} M_{\text{pl}}^2 \quad (\phi^2, N = 60) \ , \quad \lambda = 1.1 \times 10^{-12} M_{\text{pl}} \quad (\phi^3, N = 60) \ . \tag{41}
$$

Here the λ-value for the ϕ^2 potential corresponds to $m = 7.8 \times 10^{-6} M_{\text{pl}}$ ($N = 50$) and $m = 6.5 \times 10^{-6} M_{\text{pl}}$ ($N = 60$). The $V \propto \phi$ and $V \propto \phi$ models can be calculated similarly. The potential of those four models are plotted together with the reconstructed potential in Fig. 4.

As one can observe from the figures, the $V \propto \phi$ model falls outside the 2σ range of reconstructed potential (in almost whole plotted range with small α_{s}, and when the higher derivatives not yet become dominate with large α_{s}). While the $\lambda\phi^4$ model stays at the boundary of 2σ at small $\Delta\phi$. This is consistent with the n_{s}-r or ϵ-η contours in the Fig. 1. On the other hand, our approach is delightful that we now directly have the form and variance of the potential.

VI. CONCLUSION AND DISCUSSION

We have reconstructed the inflationary potential locally around a value ϕ_*, which corresponds to the time when the $\ell \simeq 50 \sim 100$ modes exits the horizon. The distribution of the inflationary slow-roll parameters (which are defined

through the expansion) are calculated, and converted to derivatives of the inflationary potential.

Two different assumptions have been tested against the reconstruction – a (theoretically) small and negligible running of the spectral index α_s, and an observationally allowed α_s from current constraints. For the case of small and negligible α_s, the reconstructed potential is highly linear over $\Delta\phi \sim M_{\rm pl}$ range. The effective field theory is practically fine (although still theoretically challenged). However, for the large α_s case, higher derivative corrections to the potential quickly dominates while ϕ rolls, which implies the inflaton keeps switching between different effective field theories, or there is a need of a tuned inflaton field theory.

With the new observational window as shown by BICEP2 data [5], much works are left to be done to accurately reconstruct the amplitude and shape of the inflation potential. Here we fit the (n_s, r) diagram with the multi-variant Gaussian distribution. We find that with current constraints from $Planck$+WP+highL+BICEP2 data, the $V(\phi) \sim \phi^2$ and ϕ^3 models are consistent within 95.4% CL, while ϕ potential is ruled out at around 99.7% CL, and ϕ^4 model is consistent within 95.4% CL if the number of e-folds is around 60. This is of-course, not a global fitting of the inflationary prediction, but constitutes a quick examination of the consistency between models and data.

It is also important to examine the theoretical assumption of the shape of gravitational wave spectra. For example, if parity is violated, which results in different amplitudes for the two tensor modes. Another example would be non-Gaussianly distributed tensor modes. It remains interesting to see whether the different theoretical models can fit the new data of CMB polarization.

Theoretically, the super-Planckian range of ϕ motion poses serious challenge to the field theory of inflation. It is very important to see how to obtain theoretical naturalness for large field inflation. Alternatively, it remains an open question that if other sources of gravitational waves, instead of the tensor fluctuation from the vacuum, could change the predictions.

[1] A. H. Guth, Phys. Rev. D. 23 (1981) 347
[2] A. D. Linde, Phys. Lett. B. 108 (1982) 38
[3] G. Hinshaw et al., 2013, ApJS, 208, 19
[4] P. A. R. Ade et al., Planck 2013 results XVI., arXiv: 1303.5076
[5] P. A. R. Ade *et al.* [BICEP2 Collaboration], arXiv:1403.3985 [astro-ph.CO].
[6] W. Zhao, C. Cheng and Q. -G. Huang, arXiv:1403.3919 [astro-ph.CO];
[7] T. Higaki, K. S. Jeong and F. Takahashi, arXiv:1403.4186 [hep-ph];
[8] K. Nakayama and F. Takahashi, arXiv:1403.4132 [hep-ph];
[9] D. J. E. Marsh, D. Grin, R. Hlozek and P. G. Ferreira, arXiv:1403.4216 [astro-ph.CO].
[10] J. E. Austermann et al., 2012, SPIE, 8452, 1
[11] N. D. Niemack et al., 2010, SPIE, 7741, 51
[12] J. R. Eimer et al., 2012, SPIE, 8452, 20
[13] P. A. R. Ade et al., arXiv: 1403.2369 [astro-ph.CO]
[14] P. A. R. Ade et al., Planck 2013 results XXII, arXiv: 1303.5082
[15] D. H. Lyth, 1997, Phys. Rev. Lett. **78**, 1861 [hep-ph/9606387].
[16] S. Hotchkiss, A. Mazumdar and S. Nadathur, 2012, JCAP **1202**, 008 [arXiv:1110.5389 [astro-ph.CO]].
[17] R. Keisler et al., 2011, ApJ, 743, 2
[18] S. Das et al., 2011, ApJ, 729, 6
[19] E. J. Copeland, A. R. Liddle, D. H. Lyth, E. D. Stewart and D. Wands, 1994, Phys. Rev. D **49**, 6410 [astro-ph/9401011].
[20] E. J. Copeland, E. W. Kolb, A. R. Liddle and J. E. Lidsey, 1993, Phys. Rev. D **48**, 2529 [hep-ph/9303288].
[21] J. E. Lidsey, A. R. Liddle, E. W. Kolb, E. J. Copeland, T. Barreiro and M. Abney, 1997, Rev. Mod. Phys. **69**, 373 [astro-ph/9508078].
[22] I. Ben-Dayan, & R. Brustein, 2010, JCAP, 09, 007
[23] P. A. R. Ade *et al.* [Planck Collaboration], arXiv:1303.5082 [astro-ph.CO].
[24] Y. Wang, arXiv:1303.1523 [hep-th].